Electronic supplementary information:

In-situ Mass Spectrometry Combined with APCVD for Mechanistic Studies of Direct N-Doped Graphene Synthesis Using Acetonitrile

Limin Wang [a, b]†,Xi Wu[c]†, Tao Cheng [b]†, Han Xue[b], Bernd Abel[d], Jia Li[c*], Jianfeng Li[b*], Liying Ma[e], Jia Ding[e], Wenqi Wang[b], Yong Hou[b], Kailang Wang[b], and Xubin Lu[b*]

[a]School of Mechanical Engineering, Lanzhou Jiaotong University, Lanzhou 730070, China.

[b]School of Materials Science and Engineering, Lanzhou Jiaotong University, Lanzhou 730070, PR China.

[c]Laboratory for Computational Materials Engineering, Division of Energy and Environment, Graduate School at Shenzhen, Tsinghua University, Shenzhen 518055, P. R. China.

[d]Institute of Chemical Technology, Leipzig University, Linnestrasse 3, 04103, Leipzig, Germany.

Key Laboratory of Advanced Ceramics and Machining Technology (Ministry of Education), [e]School of Material Science and Engineering, Tianjin University, Tianjin 300072, China.

† These authors contributed equally to this work.

E-mail: xubin.lu@lzjtu.edu.cn

E-mail: michael.bron@chemie.uni-halle.de

E-mail: li.jia@sz.tsinghua.edu.cn

E-mail: ljfpyc@163.com

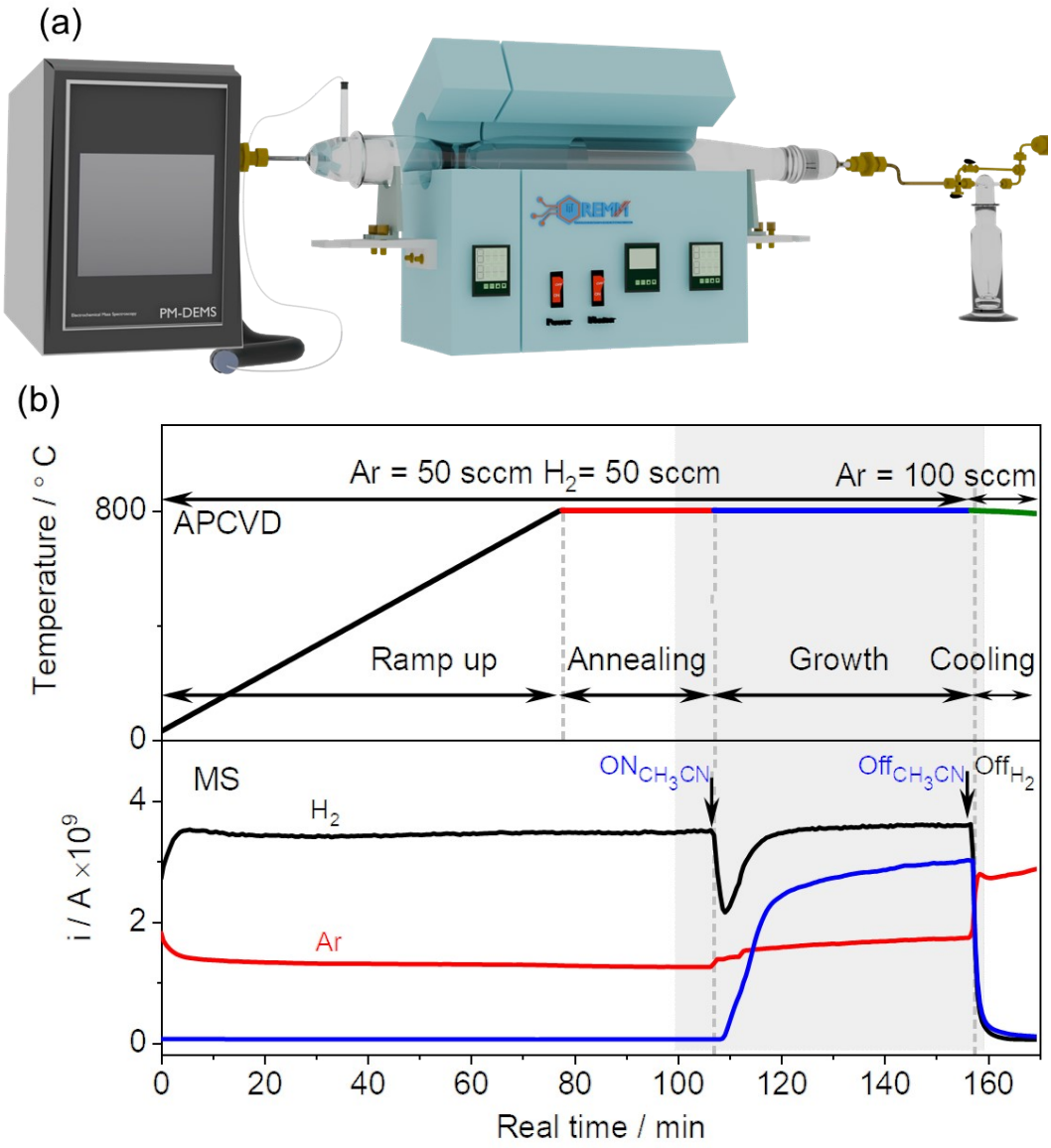

Figure S1. (a) The setup of atmospheric chemical vapor deposition (APCVD) combined with mass spectrometry (MS). Species are flowed into MS after decomposing with the APCVD, where the flow of gases and temperature are controlled through the computer terminal and the APCVD, respectively. (b) APCVD-MS plot of growth N-doped graphene at growth temperature (T_S) was set to 800 °C, the growth time (t_G) was set to 50 min. Real-time evolution of species vs the ion current changes during the ramp-up, annealing, growth and cooling stage. The analysis data was selected in the grey section, covering annealing, growth, and cooling stage.

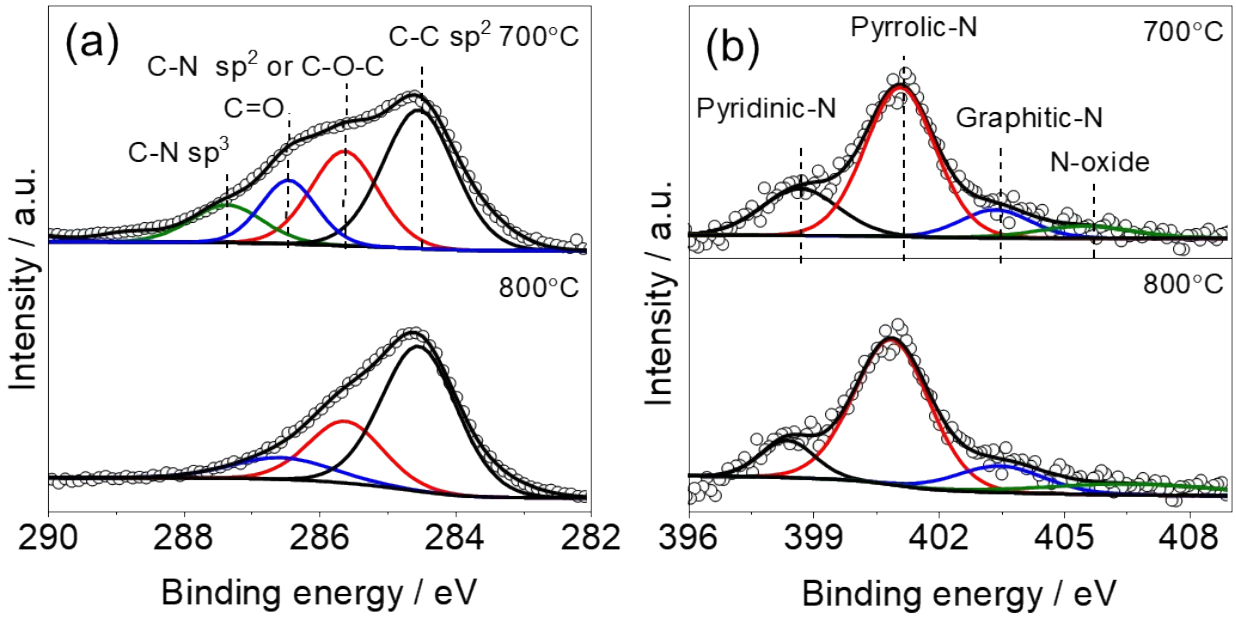

Figure S2. XPS high-resolution spectra of N-doped graphene on the Cu foil. (a) C 1 s, (b) N 1 s. The t_G = 50 min.

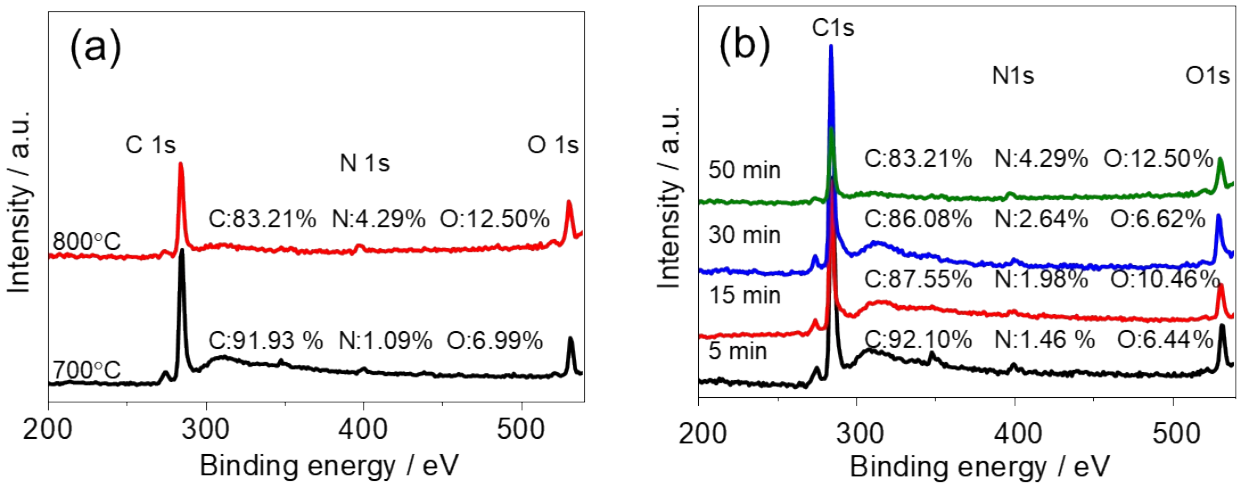

Figure S3. The central element XPS survey spectra of the N-doped graphene on the Cu substrate. (a) T_S = 700 °C and 800 °C, t_G = 50 min. (b) T_S = 800 C, t_G = 5, 15, 30, and 50 min.

Table S1. The peak positions of each N type.

	Pyridinic-N	Pyrrolic-N	Graphitic-N	N-oxide
	398.67±0.01 eV	400.47 ± 0.1 eV	401.57 ± 0.2 eV	403.57 ± 0.3 eV
5 min	18.52 %	47.63 %	19.92 %	13.93 %
15 min	16.86 %	37.85 %	35.84 %	9.45 %
30 min	24.91 %	25.25 %	24.99 %	24.85 %
50 min	10.56 %	11.72 %	64.10 %	13.62 %

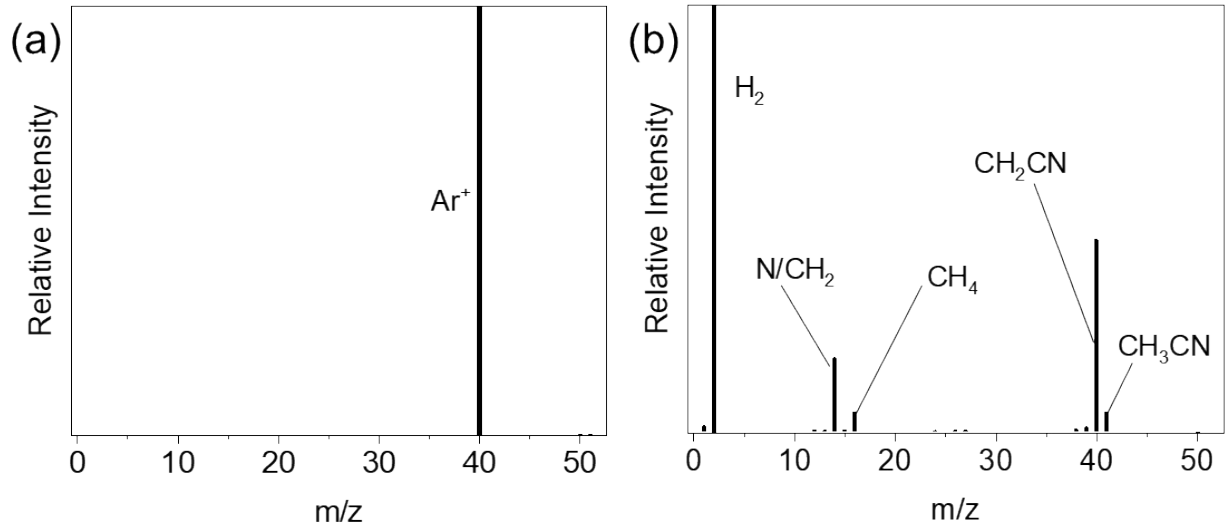

Figure S4. MS of the ions at: (a) before and (b) after injection of CH_3CN and H_2 at room temperature.

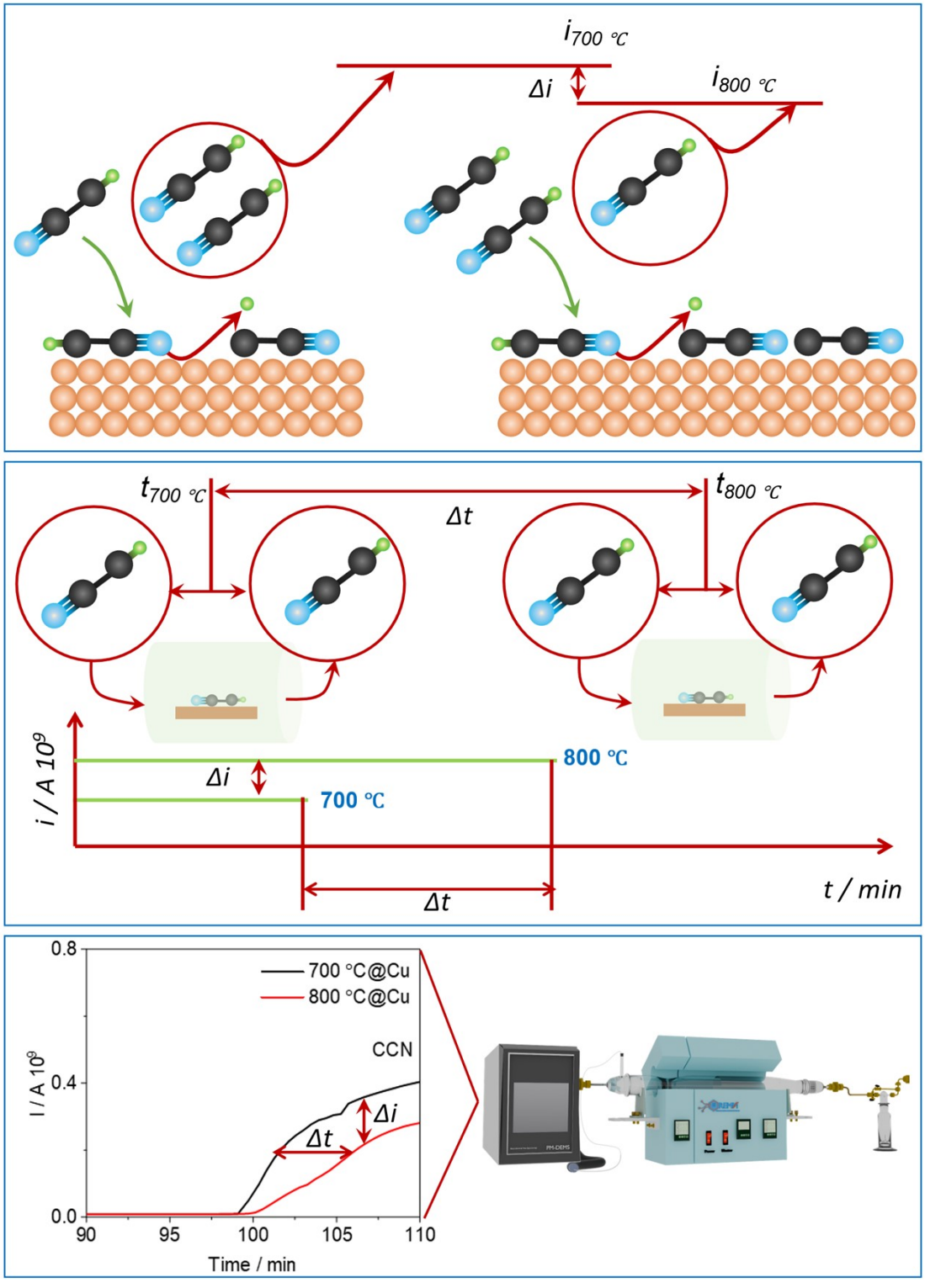

Figure S5. The illustrates the derivations of Δi and Δt..

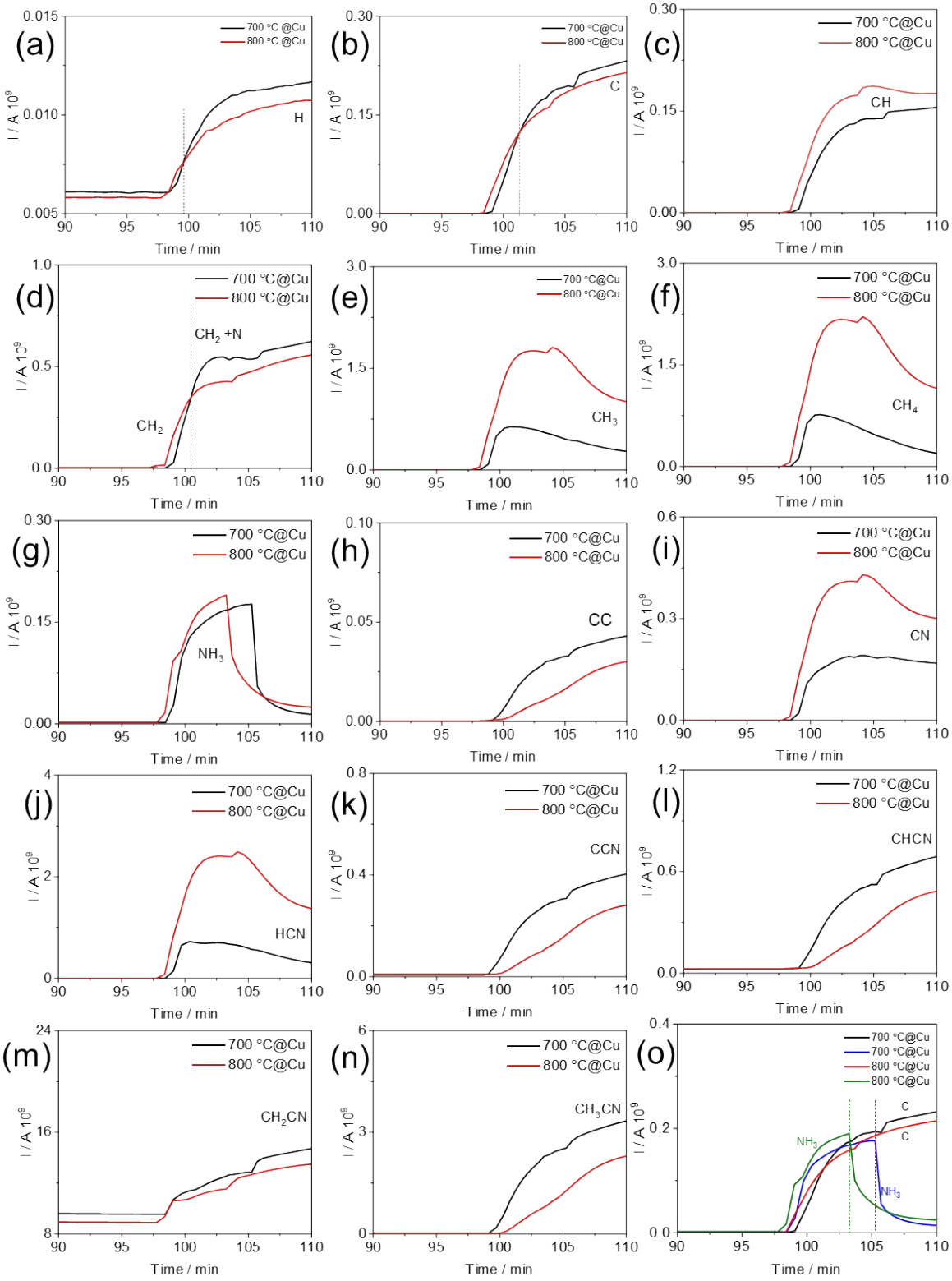

Figure S6. Real-time evolution of H, C, CH, CH_2, N, CH_3, CH_4, NH_3, CC, CN, HCN, CCN, CHCN, CH_2CN, CH_3CN, and NH_3 under 700 °C and 800 °C, respectively.

Table S2. Difference values of ion current and time-lag of detected species according to equations (1 – 4). The Δt_1 and Δt_2 of hydrogen were selected the downward shown in **Figure 3a** and **b**. (* CH_2 was calculated before decomposing 5 min, the C and N were calculated after decomposing 5 min.)

Chemical formula	Atomic mass	Δi	Δt
H^+	1	>0	<0
H_2	2	>0	<0
*C	12	>0	<0
CH	13	>0	>0
*CH_2	14	>0	>0
*N	14	>0	<0
CH_3	15	<0	<0
CH_4	16	<0	<0
NH_3	17	<0	<0
CC	24	>0	<0
CN	26	<0	>0
HCN	27	<0	>0
CCN	38	>0	<0
CHCN	39	>0	<0
CH_2CN	40	>0	<0
CH_3CN	41	>0	<0

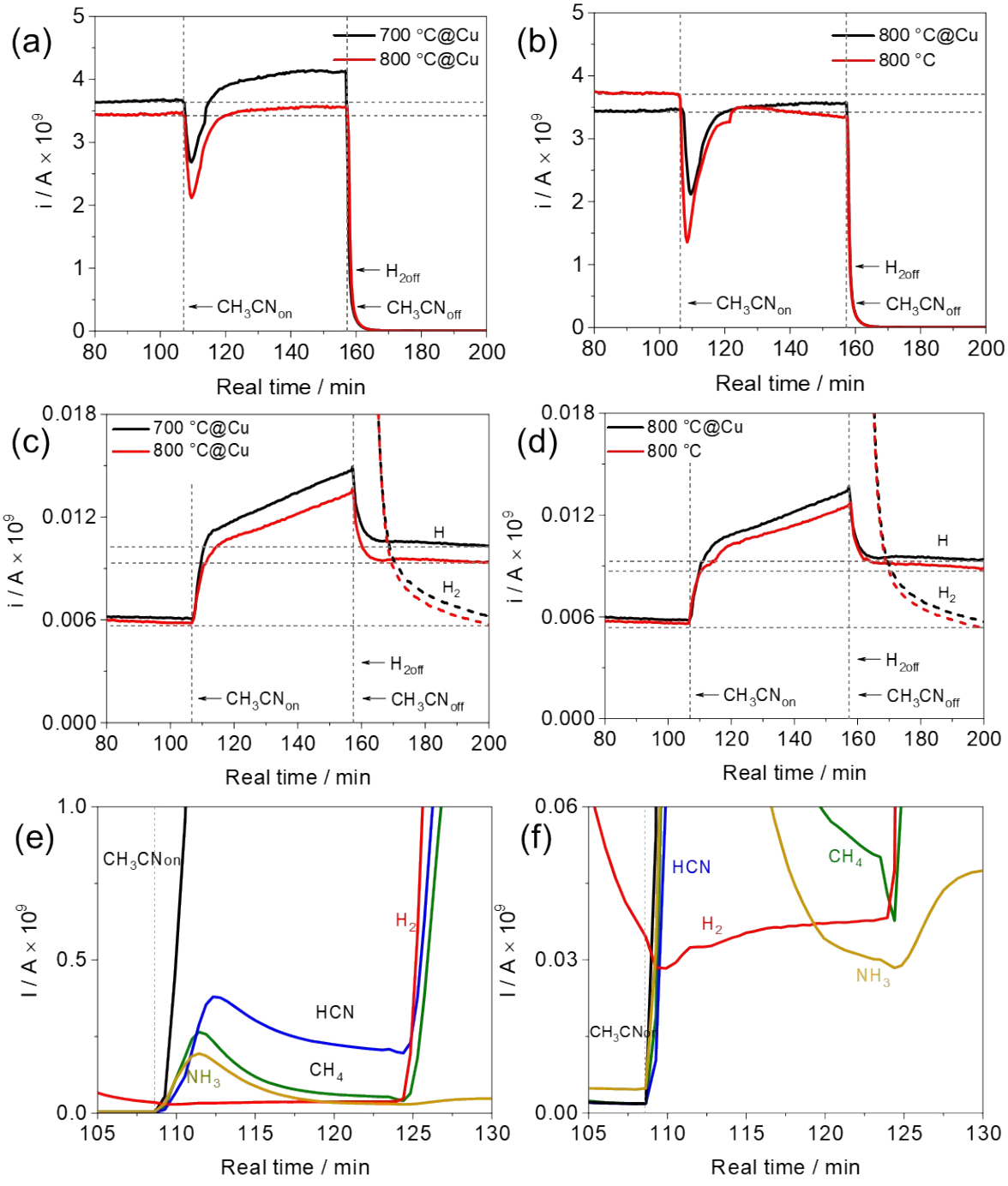

Figure S7. Real-time evolution of molecular H_2 and proton. (a, c) Growth of N-doped graphene over the Cu substrate at T_S = 700 °C and T_S = 800 °C, and t_G = 50 min. (b, d) Pyrolysis of CH_3CN at T_S = 800 °C and t_G = 50 min compared with growth of N-doped graphene on the Cu foil at the same condition. (e–f) the main products before injecting H_2 with Cu, T_S = 800 °C.

Table S3. Reaction scheme for the growth of N-doped graphene or pyrolysis of CH_3CN

	Reaction	Source
1	$H_2 + 2(s) \rightarrow H(s) + H(s)$	1, 2
2	$H(s) + H(s) \rightarrow H_2 + 2(s)$	1, 2
3	$CH_3CN \rightarrow CH_2CN + H$	3-5
4	$CH_3CN + H \rightarrow CH_3 + HCN$	3, 5
5	$CH_3CN + CH_3 \rightarrow CH_4 + CH_2CN$	3, 5
6	$CH_3CN + H \rightarrow H_2 + CH_2CN$	3, 5
7	$CH_2CN + H \rightarrow CH_2 + HCN$	3, 5
8	$CH_3CN + CN \rightarrow CH_2CN + HCN$	3, 5
9	$CH_4 + Ar \rightarrow CH_3 + H + Ar$	3, 5
10	$CH_4 + H \rightarrow CH_3 + H_2$	3, 5
11	$HCN + Ar \rightarrow H + CN + Ar$	3, 5
12	$CN + H_2 \rightarrow HCN + H$	3, 5
13	$CN + HCN \rightarrow C_2N_2 + H$	3, 5
14	$CN + CH_4 \rightarrow HCN + CH_3$	3, 5
15	$CH_4 \rightarrow CH_3 + H$	3, 6-8
16	$CH_3 \rightarrow CH_2 + H$	3, 6-8
17	$CH_2 \rightarrow CH + H$	3, 6-8
18	$CH \rightarrow C + H$	3, 4, 6-8
19	$CH_2CN \rightarrow CHCN + H$	This work
20	$CHCN \rightarrow CCN$	This work
21	$C + C \rightarrow CC$	This work

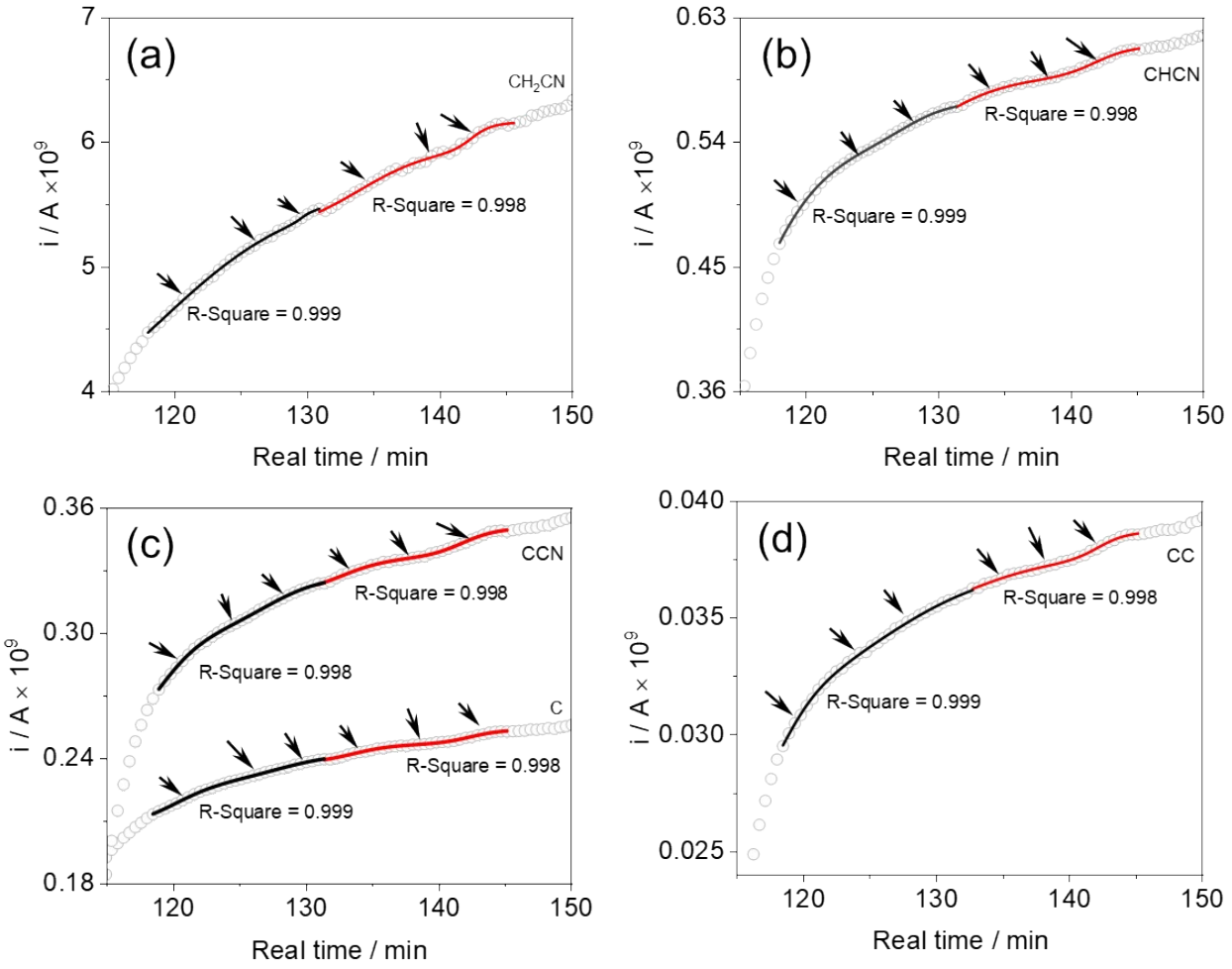

Figure S8. Real-time evolution of main radicals during the growth of graphene and/or N-doped graphene over the Cu substrate at T_S = 800 °C, and t_G = 50 min. (a) CH_2CN, (b) CHCN, (c) CCN and C, and (d) CC. The dash lines are fit for the real-time evolution of various species, Solid curves indicate Gompertz fitting to evolution of various species.

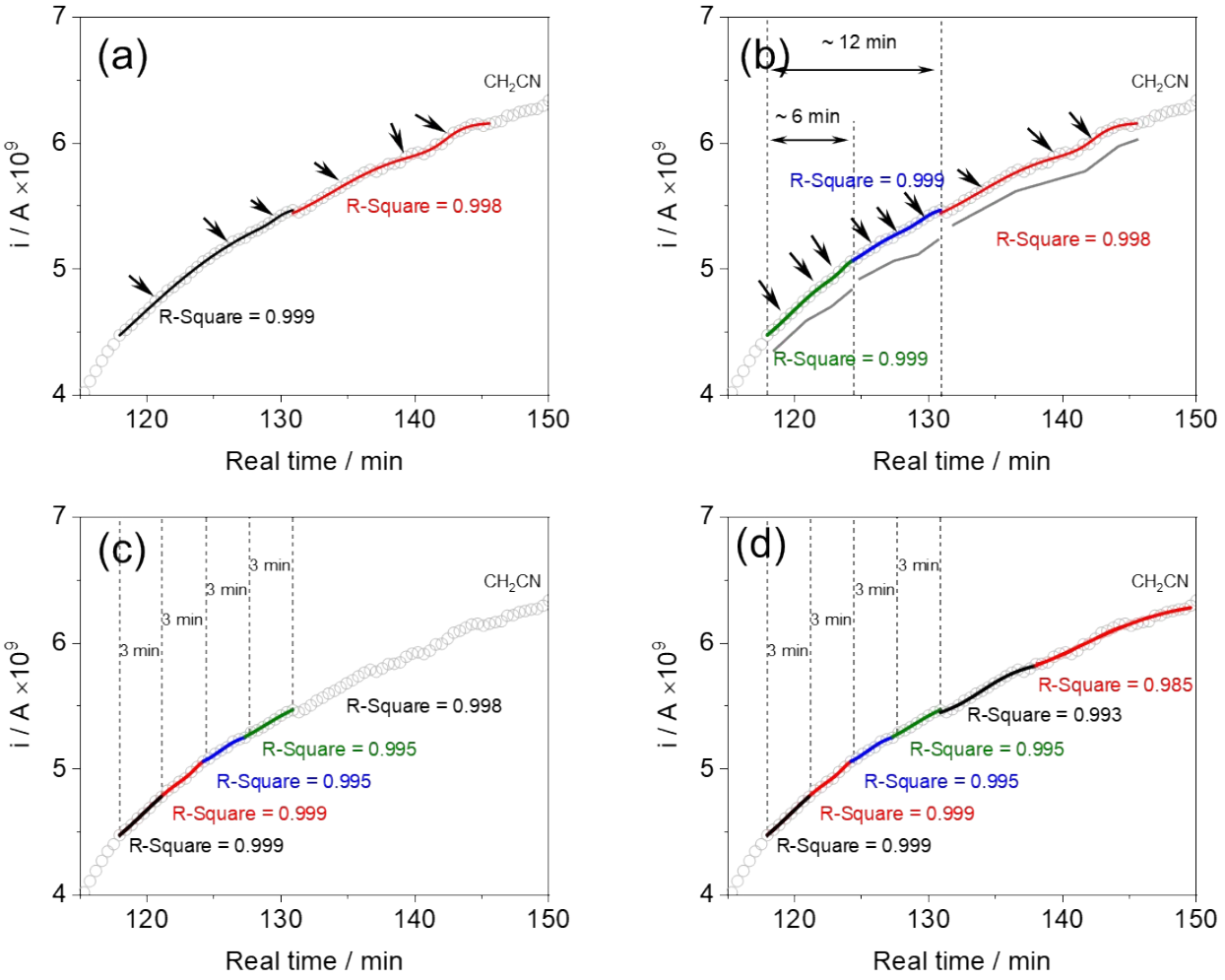

Figure S9. Fitting the real-time evolution of CH_2CN with Gompertz fitting in various time range. (a) The space of time is 12 min when the real time change from 119 min to 130 min. (b) The space of time is 6 min when the real time change from 119 min to 130 min. (c) The space of time is 3 min when the real time change from 119 min to 130 min. (d) The space of time is 3 min when the real time change from 119 min to 130 min. The space of time is gradually increase with real-time evolution after 130 min.

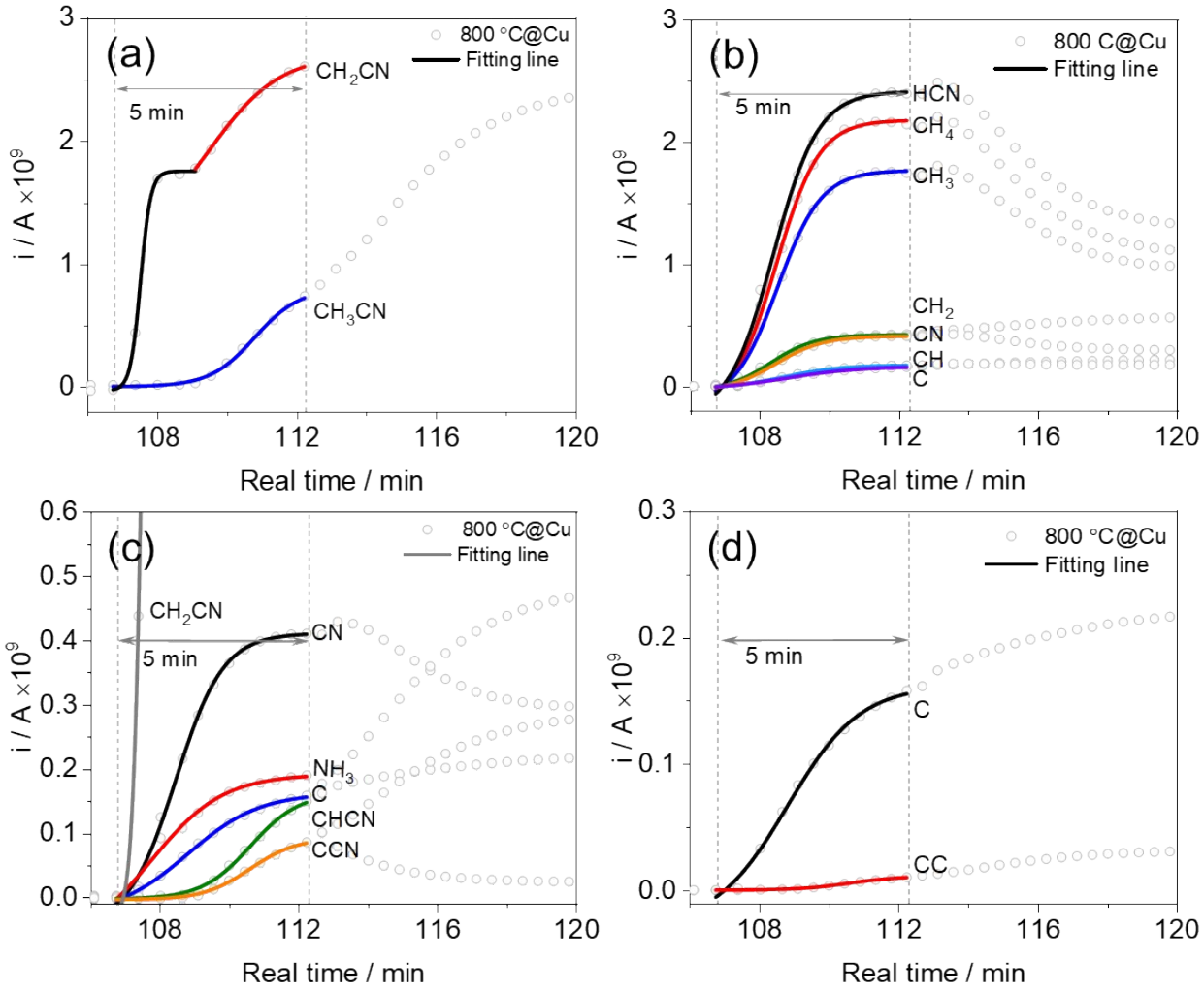

Figure S10. Real-time-lag relationship of decomposing species during the growth of graphene and/or N-doped graphene over the Cu substrate at T_S = 800 °C, and t_G = 50 min. (a) CH_3CN and main radical CH_2CN, (b) Main products HCN, CH_4 and its secondary products, (c) Probable species of forming N-doped graphene, and (d) C and CC. The dash lines are fit for the real-time evolution of various species with Gompertz fitting.

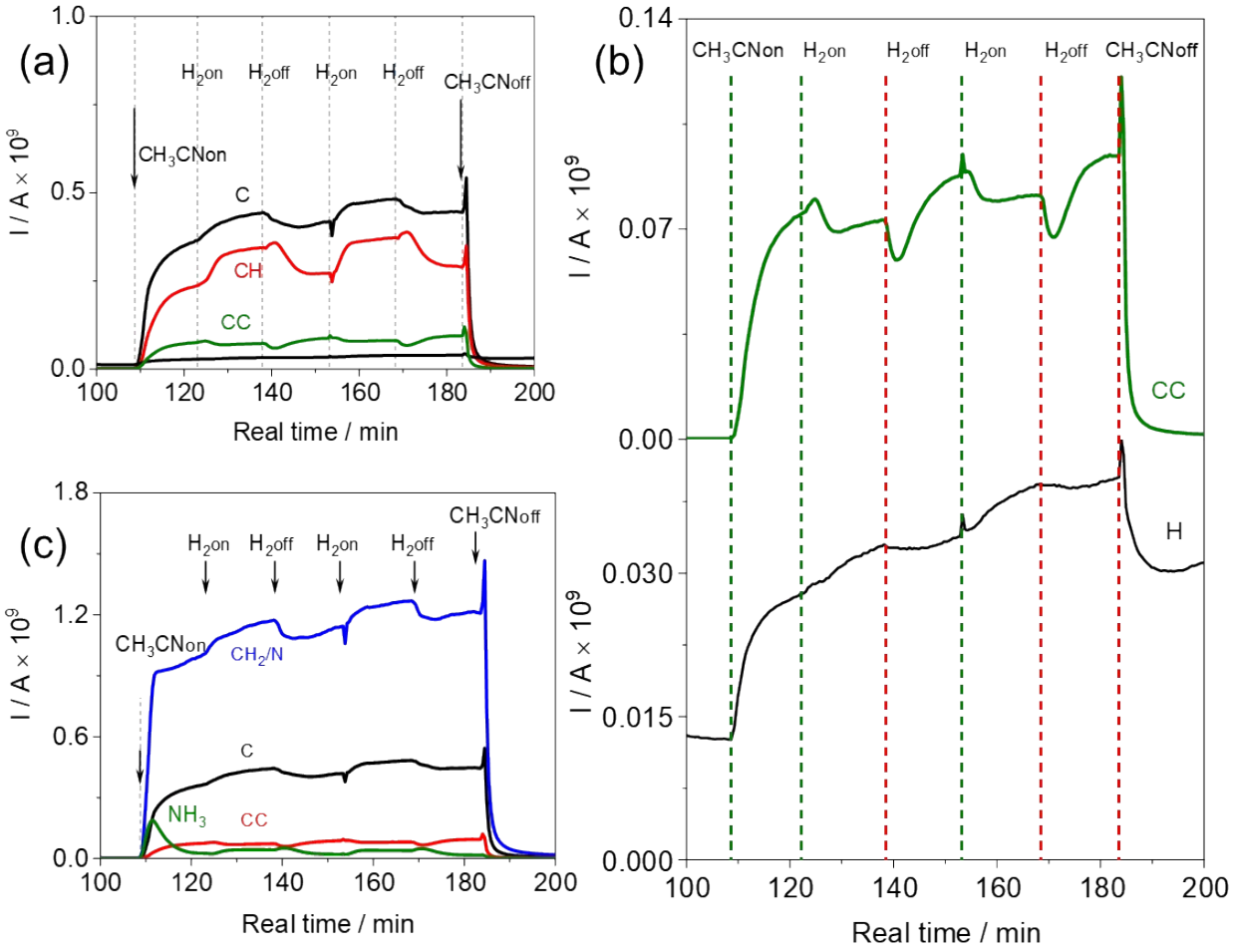

Figure S11. Real-time evolution of C, CH, CC, H, CH_2/N, and NH_3 with pulse periodic injection of H_2, T_S = 800 °C. Ar = 50 sccm, H_2 = 50 sccm. The total pressure is 1 atm.

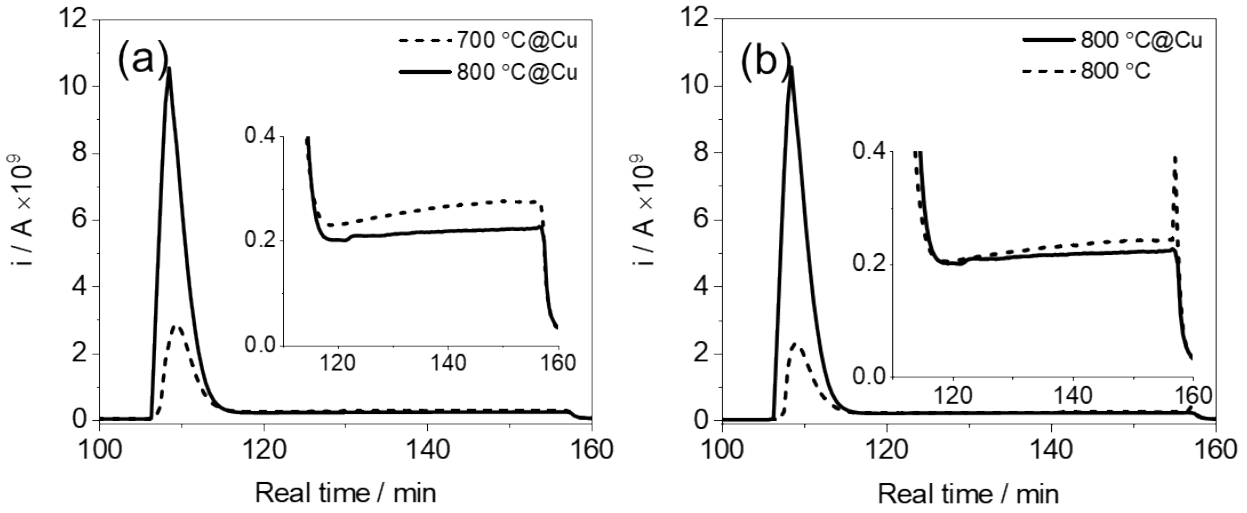

Figure S12. Real-time evolution of C_2H_4. (a) Growth of graphene and/or N-doped graphene over the Cu substrate at T_S = 700 °C, T_S = 800 °C, and t_G = 50 min. (b) Pyrolysis of CH_3CN analyzed compared with growth of NG at T_S = 800 °C, and t_G = 50 min.

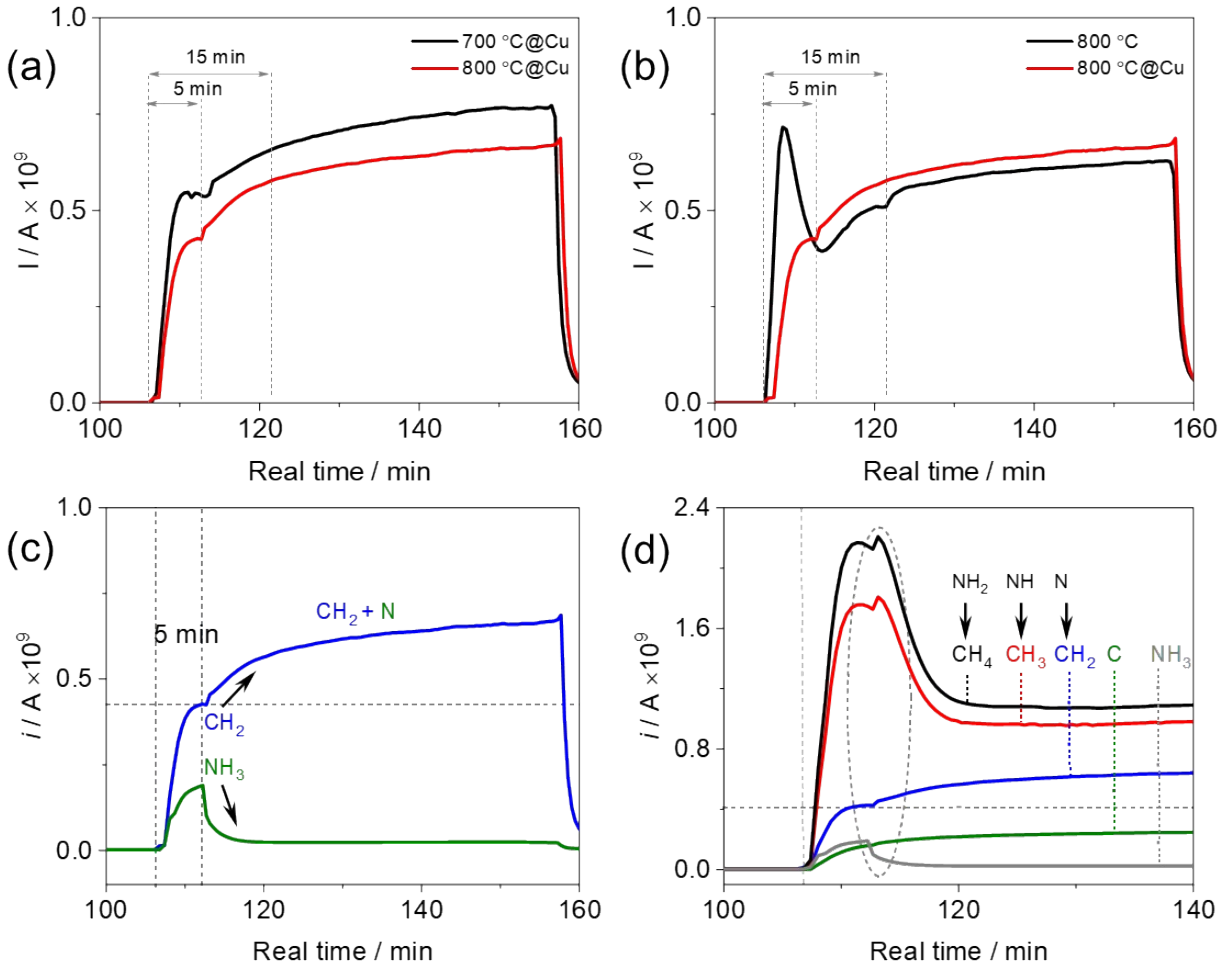

Figure S13. Real-time evolution of CH_2, NH_3, and N. (a) Growth of N-doped graphene over the Cu substrate at T_S = 700 °C and T_S = 800 °C, and t_G = 50 min. (b). Growth of NG with and without Cu substrate at T_S = 800 °C, and t_G = 50 min. (c, d) Real-time evolution of NH_3, CH_2, NH_3, CH_4, CH_3, CH_2, C (CH ≈ C). Where the growth of N-doped graphene over the Cu substrate at T_S = 800 °C, and t_G = 50 min.

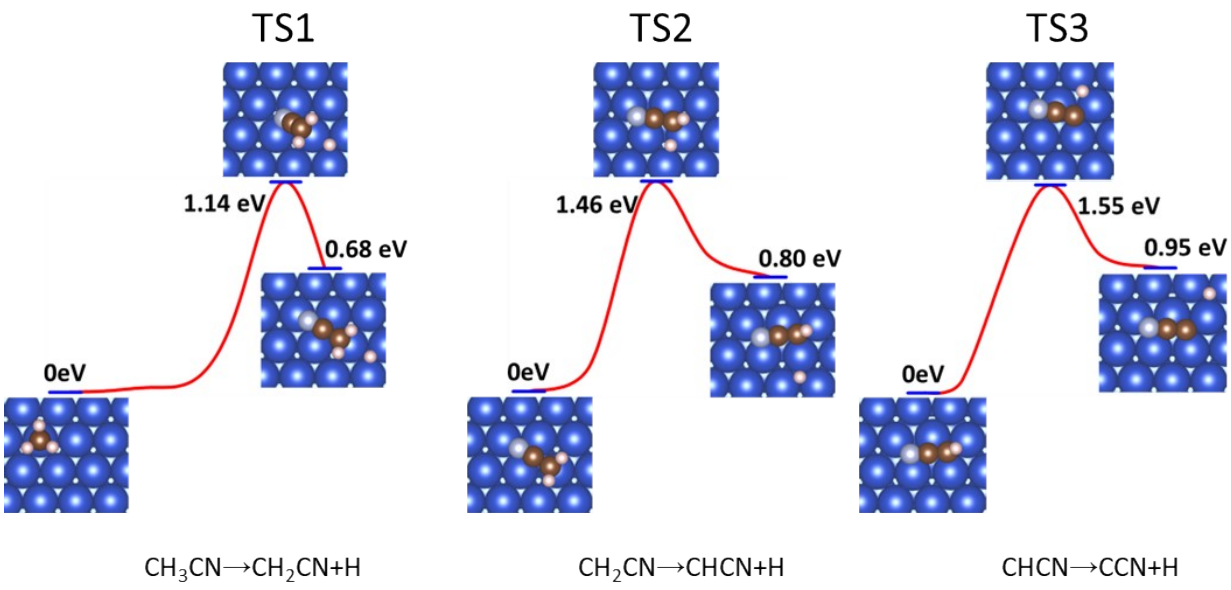

Figure S14. The geometric structure and barrier of CH_3CN dehydrogenation on Cu (111) surface. Blue, pink, gold and grey spheres represent Cu, H, C and N atoms, respectively.

TS1: CH_3CN (s) → CH_2CN (s) + H (s) and TS1*: CH_4 (s) → CH_3 (s) + H (s)

The CH_3CN molecule dissociates on the Cu surface to form a CH_2CN molecule and an H atom. In the TS1 shown in the **Figure S12**, the CH_2CN fragment adsorbs on the Cu atom with N-Cu bond, the adsorption energy is about -1.02 eV. We didn't consider the distance between C and Cu (d_{C-Cu}). The activation energy for the C-H bond cleavage was 1.14 eV, and the reaction was endothermic (ΔH = +0.68 eV) in the TS1 step. The CH_4 molecule dissociates to form a CH_3 molecule and an H atom at the TS1* step, the value of E_{act} was higher than the value of acetonitrile (E_{act} = 1.43 eV, ΔH = 0.55 eV). The value of E_{act} obtained from our calculations was lower than those calculated by Kokalj et al. [9] and Pao et al [1]. (By ~0.24 and ~0.14 eV, respectively), as shown in **Figure 6**.

TS2: CH_2CN (s) → CHCN (s) + H(s) and TS2*: CH_3 (s) → CH_2 (s) + H (s)

The starting and final structures of our CI-NEB calculation for the dissociation of CH_2CN were the CH_2CN molecule adsorbed at the Cu (111) sites (**Figure S12** TS2) and the CHCN and H species adsorbed at the Cu (111) surface. The reaction was endothermic (ΔH = +0.80 eV; E_{act} = +1.46 eV). The CH_3 were the CH_3 molecule adsorbed at the Cu fcc sites and CH_2 and H species adsorbed at the Cu (111) surface. Again, the activation energy calculated in our study (ΔH = +0.84 eV; E_{act} = +1.32 eV) was lower than those reported by Kokalj et al. and Pao et al.

TS3: CHCN (s) → CCN (s) + H (s) and TS3*: CH_2 (s) → CH (s) + H (s)

For CH_3CN, the largest energy barrier of kinetics presents the step from GS3 to TS3 (E_{act} = +1.55 eV, ΔH = +0.95eV), namely the rate-determining step. Compared with CH_4, the activation energy for the C-H bond cleavage was 0.96 eV and the reaction were endothermic (ΔH = +0.57 eV) in the TS3 step. The dissociation of CH_3CN has completed and transformed into the inert intermediate for contributing N-doped graphene, CCN.

TS4: CH (s) → C (s) + H (s)

In this step, the CH (s) underwent an upmost kinetics energy barrier, E_{act} = +1.87 eV. Finally, the CH molecule dissociates to form a C atom and an H atom, and the reaction was endothermic (ΔH = +0.95 eV). As we know, the C species are the vital intermediate of forming graphene by the conversion to CC dimers.

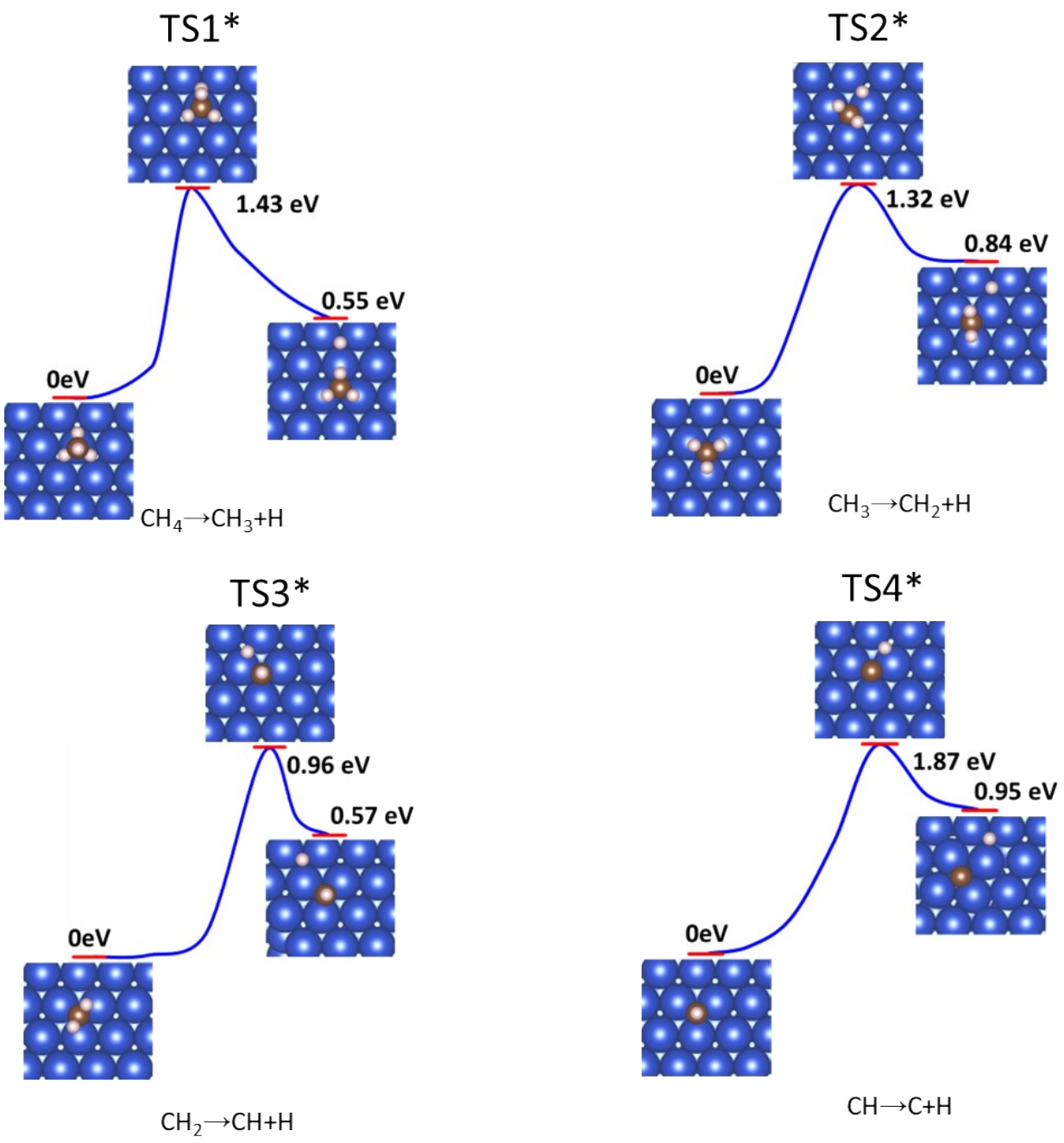

Figure S15. The geometric structure and barrier of CH_4 dehydrogenation on Cu (111) surface. Blue, pink, gold and grey spheres represent Cu, H, C and N atoms, respectively.

Table S4. Reaction energy with Cu (111)

Reactant		Product	E_R	E_P	ΔE
CH_3CN	→	CH_3+CN	-37.36	-36.93	0.43
CH_3CN	→	CH_2CN+H	-37.36	-36.89	0.47
H+CH_3CN	→	CH_4+CN	-41.05	-41.18	-0.13
H+CH_3CN	→	CH_3+HCN	-41.05	-40.07	0.98
2H+CH_3CN	→	CH_4+HCN	-44.74	-44.32	0.42
2H+CH_3CN	→	CH_3CH+NH	-44.74	-43.89	0.85
CH_2CN	→	CH_2+CN	-33.2	-32.43	0.77
CH_2CN	→	CHCN+H	-33.2	-32.33	0.87
H+CH_2CN	→	CH_3+CN	-36.89	-36.93	-0.04
H+CH_2CN	→	CH_2+HCN	-36.89	-35.57	1.32
2H+CH_2CN	→	CH_3+HCN	-40.58	-40.07	0.51
CHCN	→	CH+CN	-28.64	-28.3	0.34
CHCN	→	CCN+H	-28.64	-27.65	0.99
H+CHCN	→	CH_2+CN	-32.33	-32.43	-0.1
H+CHCN	→	CH+HCN	-32.33	-31.44	0.89
2H+CHCN	→	CH_2+HCN	-36.02	-35.57	0.45
CCN	→	C+CN	-23.96	-23.38	0.58
CCN	→	CC+N	-23.96	-22.72	1.24
H+CCN	→	CH+CN	-27.65	-28.3	-0.65
H+CCN	→	C+HCN	-27.65	-26.52	1.13
2H+CCN	→	CH+HCN	-31.34	-31.44	-0.1
H_2	→	2H	-6.86	-7.38	-0.52
HCN	→	H+CN	-20.03	-20.58	-0.55
CN	→	C+N	-16.89	-13.42	3.47
H+CN	→	CH+N	-20.58	-18.34	2.24
H+CN	→	C+NH	-20.58	-18.36	2.22
2H+CN	→	CH+NH	-24.27	-23.28	0.99
CC	→	2C	-15.79	-12.98	2.81
H+CC	→	C+CH	-19.48	-17.9	1.58
2H+CC	→	2CH	-23.17	-22.82	0.35
CH_4	→	CH_3+H	-24.29	-23.73	0.56
CH_3	→	CH_2+H	-20.04	-19.23	0.81
CH_2	→	CH+H	-15.54	-15.1	0.44
CH	→	C+H	-11.41	-10.18	1.23
NH_3	→	NH_2+H	-20.37	-19.84	0.53
NH_2	→	NH+H	-16.15	-15.56	0.59
NH	→	N+H	-11.87	-10.62	1.25

Table S5. Reaction energy without Cu (111).

Reactant		Product	E_R	E_P	ΔE
CH_3CN	→	CH_3+CN	-36.73	-30.71	6.02
CH_3CN	→	$CH_2CN+1/2H_2$	-36.73	-34.33	2.4
$1/2H_2+CH_3CN$	→	CH_4+CN	-40.11	-36.55	3.56
$1/2H_2+CH_3CN$	→	CH_3+HCN	-40.11	-37.88	2.23
H_2+CH_3CN	→	CH_4+HCN	-43.49	-43.72	-0.23
H_2+CH_3CN	→	CH_3CH+NH	-43.49	-34.86	8.63
CH_2CN	→	CH_2+CN	-30.95	-24.62	6.33
CH_2CN	→	$CHCN+1/2H_2$	-30.95	-28.29	2.66
$1/2H_2+CH_2CN$	→	CH_3+CN	-34.33	-30.71	3.62
$1/2H_2+CH_2CN$	→	CH_2+HCN	-34.33	-31.79	2.54
H_2+CH_2CN	→	CH_3+HCN	-37.71	-37.88	-0.17
CHCN	→	CH+CN	-24.91	-18.72	6.19
CHCN	→	$CCN+1/2H_2$	-24.91	-22.89	2.02
$1/2H_2+CHCN$	→	CH_2+CN	-28.29	-24.62	3.67
$1/2H_2+CHCN$	→	CH+HCN	-28.29	-25.89	2.4
H_2+CHCN	→	CH_2+HCN	-31.67	-31.79	-0.12
CCN	→	C+CN	-19.51	-13.78	5.73
CCN	→	CC+N	-19.51	-9.06	10.45
$1/2H_2+CCN$	→	CH+CN	-22.89	-18.72	4.17
$1/2H_2+CCN$	→	C+HCN	-22.89	-20.95	1.94
H_2+CCN	→	CH+HCN	-26.27	-25.89	0.38
H2	→	2H	-6.76	-0.02	6.74
HCN	→	$1/2H_2$+CN	-19.69	-15.9	3.79
CN	→	C+N	-12.52	-1.31	11.21
$1/2H_2+CN$	→	CH+N	-15.9	-6.25	9.65
$1/2H_2+CN$	→	C+NH	-15.9	-7.56	8.34
H_2+CN	→	CH+NH	-19.28	-12.5	6.78
CC	→	2C	-9.01	-2.52	6.49
$1/2H_2+CC$	→	C+CH	-12.39	-7.46	4.93
H_2+CC	→	2CH	-15.77	-12.4	3.37
CH_4	→	$CH_3+1/2H_2$	-24.03	-21.57	2.46
CH_3	→	$CH_2+1/2H_2$	-18.19	-15.48	2.71
CH_2	→	$CH+1/2H_2$	-12.1	-9.58	2.52
CH	→	$C+1/2H_2$	-6.2	-4.64	1.56
NH_3	→	$NH_2+1/2H_2$	-19.52	-16.16	3.36
NH_2	→	$NH+1/2H_2$	-12.78	-9.68	3.1
NH	→	$N+1/2H_2$	-6.3	-3.43	2.87

Table S6. The adsorption energy of the main intermediates in the decomposition of CH_3CN and CH_4.

	E_{tot}	E_{sub}	N_H	E	$E_{relative}$	$E_{molecole}$	E_{ads}
CH_3CN	-318.68	-281.32	0	-318.68	0	-36.73	-0.63
CH_2CN	-314.52	-281.32	1	-318.20	0.48	-30.95	-2.25
CHCN	-309.96	-281.32	2	-317.33	1.35	-24.91	-3.73
CCN	-305.28	-281.32	3	-316.34	2.34	-19.51	-4.45
H	-285.01	-281.32	---	---	---		
CH_4	-203.57	-179.28	0	-203.57	0	-24.03	-0.26
CH_3	-199.32	-179.28	1	-203.02	0.55	-18.19	-1.85
CH_2	-194.82	-179.28	2	-202.22	1.35	-12.10	-3.44
CH	-190.69	-179.28	3	-201.79	1.78	-6.20	-5.21
C	-185.77	-179.28	4	-200.57	3.00	-1.26	-5.23
H	-182.98	-179.28	---	---	---		

Table S7. The adsorption energy of decomposed species.

	E_{tot}	E_{sub}	$E_{molecole}$	E_{ads}
H_2	-288.18	-281.32	-6.76	-0.1
H	-285.01	-281.32	-0.01	-3.68
HCN	-301.35	-281.32	-19.69	-0.34
CN	-298.21	-281.32	-12.52	-4.37
CC	-297.11	-281.32	-9.01	-6.78
CH_3CH_2	-317.78	-281.32	-34.33	-2.13
CH_3CH	-313.34	-281.32	-28.56	-3.46
NH_3	-301.69	-281.32	-19.52	-0.85
NH_2	-297.47	-281.32	-12.78	-3.37
NH	-293.19	-281.32	-6.30	-5.57
N	-288.25	-281.32	-0.05	-6.88

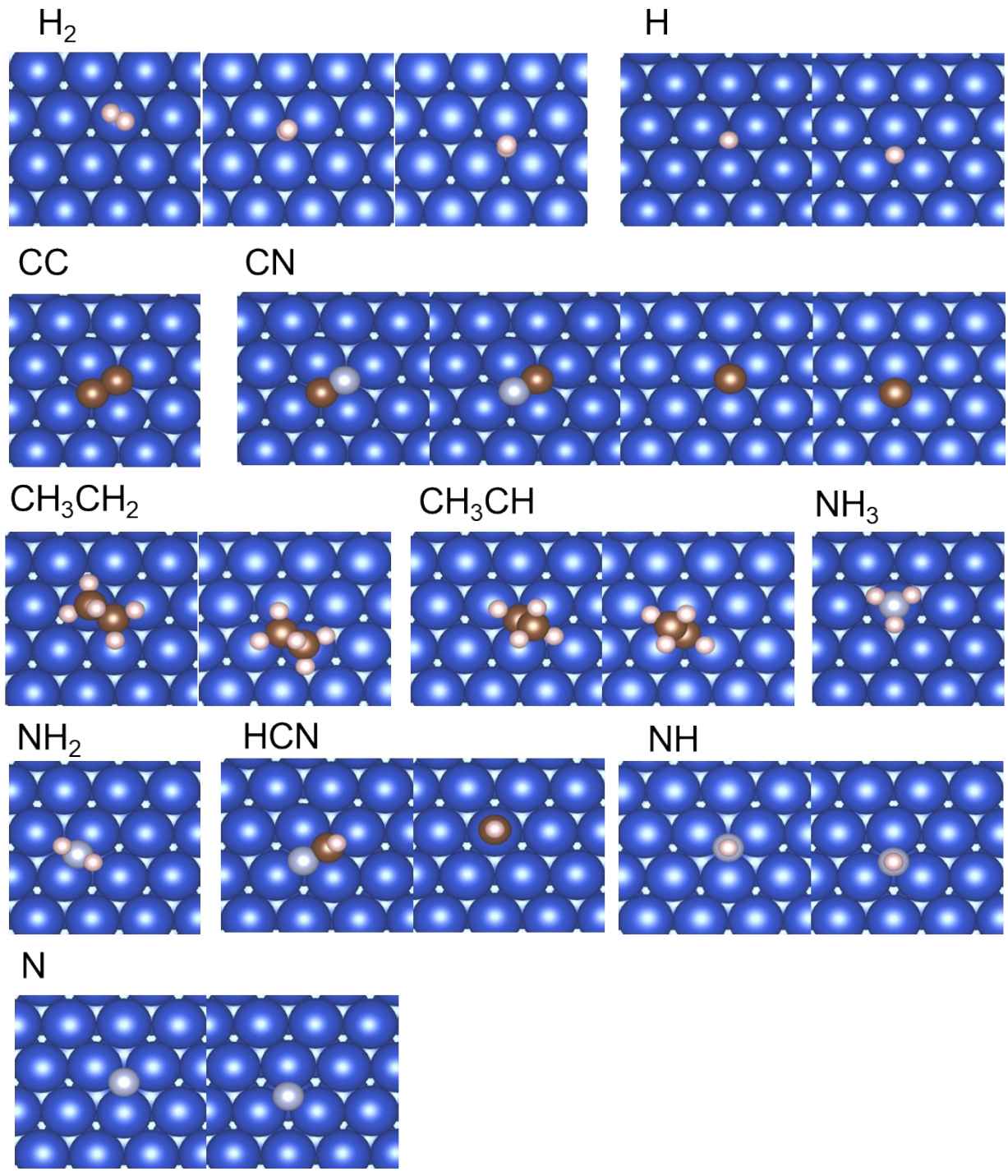

Figure S16. Geometric structures of the probable state of the relevant intermediates on Cu (111) surface. Where the first state is the lowest energy state among probable states.

Reference

1. G. Gajewski and C. W. Pao, Ab initio calculations of the reaction pathways for methane decomposition over the Cu (111) surface, *J Chem Phys*, 2011, **135**, 064707.
2. I. Vlassiouk, M. Regmi, P. Fulvio, S. Dai, P. Datskos, G. Eres and S. Smirnov, Role of Hydrogen in Chemical Vapor Deposition Growth of Large Single-Crystal Graphene, *ACS Nano*, 2011, **5**, 6069-6076.
3. A. Lifshitz, A. Moran and S. Bidani, Thermal reactions of acetonitrile at high temperatures. Pyrolysis behind reflected shocks, *International Journal of Chemical Kinetics*, 1987, **19**, 61-79.
4. A. Lifshit, Y. Cohen, M. Braun-Unkhoff and P. Frank, Thermal decomposition of benonitrile: A combined single-pulse shock tube-aras investigation, *Symposium (International) on Combustion*, 1996, **26**, 659-667.
5. A. Lifshitz and C. Tamburu, Thermal decomposition of acetonitrile. Kinetic modeling, *International Journal of Chemical Kinetics*, 1998, **30**, 341-347.
6. M. Losurdo, M. M. Giangregorio, P. Capezzuto and G. Bruno, Graphene CVD growth on copper and nickel: role of hydrogen in kinetics and structure, *Physical Chemistry Chemical Physics*, 2011, **13**, 20836-20843.
7. W. Zhang, P. Wu, Z. Li and J. Yang, First-Principles Thermodynamics of Graphene Growth on Cu Surfaces, *The Journal of Physical Chemistry C*, 2011, **115**, 17782-17787.
8. A. Kokalj, N. Bonini, C. Sbraccia, S. de Gironcoli and S. Baroni, Engineering the Reactivity of Metal Catalysts: A Model Study of Methane Dehydrogenation on Rh(111), *Journal of the American Chemical Society*, 2004, **126**, 16732-16733.
9. A. Kokalj, N. Bonini, S. d. Gironcoli, C. Sbraccia, G. Fratesi and S. Baroni, Methane Dehydrogenation on Rh@Cu(111): A First-Principles Study of a Model Catalyst, *journal of the American Chemical Society*, 2006, **128**, 12448-12454.